NJC

PAPER

View Article Online
View Journal

Cite this: DOI: 10.1039/c5nj01905b

Mimicking vanadium haloperoxidases: vanadium(III)–carboxylic acid complexes and their application in H_2O_2 detection†

Xiao Dong Feng,[a] Xiao Xi Zhang,[a] Zhi Nan Wang,[a] Jian Song,[a] Yong Heng Xing*[a] and Feng Ying Bai*[b]

Received (in Montpellier, France) 21st July 2015,
Accepted 10th November 2015

DOI: 10.1039/c5nj01905b

www.rsc.org/njc

Vanadium(III) complexes $[V(2,6\text{-pdc})_2(H_2O)_2]\cdot 2H_2O$ (**1**) and $V(2,6\text{-pdc})(htba)(H_2O)_2$ (**2**), (2,6-pdc = 2,6-pyridinedicarboxylic acid, htba = 2-acetoxy-4-trifluoromethylbenzoic acid) have been synthesized by the reaction of $V_2(SO_4)_3$ with 2,6-pdc (for **1**) or 2,6-pdc and htba (for **2**) under hydrothermal conditions at 120 °C for 36 hours. Because the vanadium(III) was easily oxidized into higher oxidation states, we included the reducing agent vitamin C to protect the vanadium(III) center. The complexes were characterized by elemental analysis, IR and UV-vis spectroscopy, and single-crystal X-ray diffraction. Structural analysis revealed that the central metal V atoms in the complexes **1** and **2** were seven-coordinate, forming pentagonal bipyramid geometries. The complexes catalyzed the bromination of the organic substrate phenol red in the presence of H_2O_2, bromide and buffer. Compared with vanadium complexes having other oxidation states, the vanadium(III) complexes had better catalytic activity (the maximum reaction rate constant was 2.424×10^2 k(mol $L^{-1})^{-2}$ s^{-1}). The mimicking vanadium haloperoxidases also overcame some serious disadvantages of natural enzymes. Therefore, the reaction system described herein can be considered as an effective model for hydrogen peroxide determination.

Introduction

Hydrogen peroxide is an integral part of atmospheric chemistry and biological systems. In the atmosphere, it is an oxidant that is produced from the combination of hydroperoxyl radicals ($HO_2^{\bullet}$) and their hydrated form.[1] Hydrogen peroxide is exceptionally soluble in water and it is thought to be the most efficient oxidant in the formation of H_2SO_4 from dissolved SO_2. This implies that hydrogen peroxide could have some role in the acidity of rainwater.[2] Furthermore, hydrogen peroxide is of great practical importance in the food and pharmaceutical industries and clinical and other industrial fields.[3–6] Hence, there is an urgent need to establish a convenient, effective and rapid method for the detection of H_2O_2.

There are numerous detection methods for H_2O_2,[7–14] of which the colorimetric method is one of the most popular. Others include HPLC, electrochemistry detection, chemiluminescence, *etc.*[15–20] Titanium-based assays (Ti-PAPS reagents) were developed in the 1980s for spectrophotometric detection of H_2O_2.[9] The Fox assay was developed in the 1990s based on ferrous ion oxidation in the presence of the ferric ion indicator xylenol orange under acidic conditions.[10] Recently, Luo and co-workers developed a detection method based on the oxidation of methyl orange using an iron-catalyzed Fenton reaction system under acidic conditions.[12]

Other methods, using fluorescent probes, have recently been developed to monitor hydrogen peroxide production in living cells.[13] Chemiluminescence methods have also been developed recently.[14] These methods are highly sensitive, but they are limited by the complicated apparatus setup and sensor preparation, and interference from metal ions. Based on the points above, we developed a colorimetric method to detect H_2O_2.

Vanadium haloperoxidases (V-HPOs) which are found in marine algae are able to accelerate the oxidative halogenation of organic compounds in the presence of hydrogen peroxide, organic hydroperoxides or molecular oxygen.[21–23] Unfortunately, natural enzymes are proteins and inherently bear some serious disadvantages, such as easy denaturation by environmental changes, digestion by proteases, as well as time-consuming and expensive preparation and purification. Therefore, much effort has been put into developing stable artificial enzyme mimics of vanadium complexes as functional models for V-HPOs.[24–28]

[a] College of Chemistry and Chemical Engineering, Liaoning Normal University, Huanghe Road 850#, Dalian City, 116029, P. R. China.
E-mail: xingyongheng2000@163.com; Tel: +86-411-82156987
[b] College of Life Science, Liaoning Normal University, Dalian 11602, P. R. China

† Electronic supplementary information (ESI) available: Tables of atomic coordinates, isotropic thermal parameters, and complete bond distances. CCDC 1056936 (**1**) and 1056937 (**2**). For ESI and crystallographic data in CIF or other electronic format see DOI: 10.1039/c5nj01905b

Vanadium complexes are able to mimic a reaction in which vanadium catalyzes the bromination of organic substrates in the presence of H_2O_2 and bromide.[26–31] Through experimental results, it is found that the oxidation reaction catalyzed by the vanadium complexes is H_2O_2 concentration-dependent, and the absorbance at 592 nm along with the formation of bromophenol blue presents a linear dependence on the concentration of H_2O_2. The linear dependence of absorbance on H_2O_2 concentration can be used in the detection and quantification of H_2O_2.

In order to study the functional properties of vanadium(III) complexes, here we synthesized two vanadium(III) complexes, $V(2,6\text{-pdc})_2(H_2O)_2{\cdot}2H_2O$ (**1**) and V(2,6-pdc)(htba)$(H_2O)_2$ (**2**), (2,6-pdc = 2,6-pyridinedicarboxylic acid, htba = 2-acetoxy-4-trifluoromethylbenzoic acid) and studied their bromination reaction activity and their ability to detect hydrogen peroxide.

Experimental

Materials and methods

Elemental analyses for C, H, and N were carried out on a PerkinElmer 240C automatic analyzer. The infrared spectra were recorded on a JASCO FT/IR-480 spectrometer with pressed KBr pellets in the range 200–4000 cm^{-1}. UV-vis spectra were recorded on a JASCO V-570 spectrometer (200–1500 nm, using solid samples). The X-ray powder diffraction data were collected on a Bruker AXS D8 Advance diffractometer using Cu-Kα radiation (λ = 1.5418 Å) in the 2θ range of 5–60° with a step size of 0.02° and a scanning rate of 3° min^{-1}.

Synthesis of the complexes

$[V(2,6\text{-pdc})_2(H_2O)_2]{\cdot}2H_2O$ (1). $V_2(SO_4)_3$ (0.0390 g, 0.1 mmol), 2,6-pdc (0.0334 g, 0.2 mmol) and vitamin C (0.0180 g, 0.1 mmol) were mixed and stirred for 3 h in a solution of H_2O (15 mL) at room temperature, forming a kind of yellow turbid solution (pH = 6.5). Then, the mixture was sealed into a 23 mL Teflon-lined stainless steel autoclave and heated at 120 °C. After 36 h, it was cooled to room temperature and yellow crystals suitable for X-ray diffraction were obtained. Yield (based on V): 0.0346 g, 75.14%. Anal. calc. (%). For $C_{14}H_{15}N_2O_{12}V$: C, 36.94; H, 3.33; N, 12.31. Found: C, 36.91; H, 3.36; N, 12.30.

V(2,6-pdc)(htba)$(H_2O)_2$ (2). The synthesis method of complex **2** was similar to that for complex **1**. $V_2(SO_4)_3$ (0.0390 g, 0.1 mmol), htba (0.0206 g, 0.1 mmol), 2,6-pdc (0.0167 g, 0.1 mmol) and vitamin C (0.0180 g, 0.1 mmol) were mixed and stirred for 2 h in a solution of H_2O (15 mL) at room temperature, forming a yellow turbid solution (pH = 6.5). After 1 day of heating at 120 °C, the mixture was cooled to room temperature and yellow crystals of **2** were obtained. Yield (based on V): 0.0368 g, 80.49%. Anal. calc. (%). For $C_{15}H_9NO_9F_3V$: C, 39.37; H, 1.97; N, 3.06. Found: C, 39.38; H, 1.99; N, 3.05.

X-ray single crystal structural determinations

Suitable single crystals of the two complexes were mounted on glass fibers for X-ray measurement. Reflection data were collected at room temperature with a Bruker AXS SMART APEX II CCD diffractometer (Bruker AXS, Karlsruhe, Germany) with graphite-monochromated Mo-Kα radiation (λ = 0.7107 Å) and a ω scan mode. All measured independent reflections ($I > 2\sigma(I)$) were used in the structural analysis, and semi-empirical absorption corrections were applied using the SADABS program.[32] The structures were solved by the direct method using SHELXL-97.[33] The non-hydrogen atoms were refined with anisotropic thermal parameters. Hydrogen atoms of the organic frameworks were fixed at calculated positions with isotropic thermal parameters and refined using a riding model. Crystal data and structure refinements are shown in Table 1. The selected bond lengths and bond angles are listed in Table S1 (ESI†). Hydrogen bonds of the complexes **1–2** are given in Table S2 (ESI†).

Table 1 Crystallographic data and structure refinement for complexes **1–2**[a]

Complexes	**1**	**2**
Formula	$C_{14}H_{15}N_2O_{12}V$	$C_{15}H_{11}NO_9F_3V$
M (g mol^{-1})	454.22	457.19
Crystal system	Triclinic	Monoclinic
Space group	$P\bar{1}$	$P2(1)/c$
a (Å)	8.540(2)	15.3219(17)
b (Å)	9.813(3)	17.734(2)
c (Å)	11.707(3)	6.6947(8)
α (°)	82.404(4)	90
β (°)	73.547(4)	90.641(2)
γ (°)	68.028(4)	90
V (Å^3)	872.2(4)	1818.9(4)
Z	2	4
D_{calc} (Mg m^{-3})	1.730	1.670
Crystal size (mm)	0.12 × 0.08 × 0.05 mm	0.32 × 0.24 × 0.09 mm
F(000)	464	920
μ (Mo-Kα)/mm^{-1}	0.642	0.626
θ (°)	1.81 to 25.95	1.76 to 28.44
Reflections collected	4712	11358
Independent reflections ($I > 2\sigma(I)$)	3313	4462
Parameters	262	312
$\Delta(\rho)$ (e Å^{-3})	0.690 and −0.705	0.511 and −0.467
Goodness-of-fit	1.044	1.037
R_1[a]	0.0555(0.0835)[b]	0.0387(0.0567)[b]
wR_2[a]	0.1371(0.1534)[b]	0.0975(0.1066)[b]

[a] $R = \sum||F_o| - |F_c||/\sum|F_o|$, w$R_2 = [\sum[w(|F_o|^2 - |F_c|^2)^2]/\sum[w(|F_o|^2)^2]]^{1/2}$; $[|F_o| > 4\alpha(|F_o|)]$. [b] Based on all data.

Measurement of bromination activity in solution

Each vanadium complex was dissolved in a mixed solution of 25 mL H_2O–DMF (DMF: 2 mL; H_2O: 23 mL). The reactions were initiated by the mixing of phenol red solution (10^{-4} mol L^{-1}), buffer solution of NaH_2PO_4–Na_2HPO_4 (pH = 5.8), KBr (0.4 mol L^{-1}), vanadium complex (0.1 mmol L^{-1}) and H_2O_2 (30%), and the bromination reaction activity tests were carried out at the constant temperature of 30 ± 0.5 °C. Vanadium complexes at five different concentrations (measured 0.5 mL, 1 mL, 1.5 mL, 2 mL, 2.5 mL respectively from 0.1 mmol L^{-1} vanadium complex) were placed in five cuvettes, and then put into the constant temperature water bath. The spectral changes were recorded using a UV1000 spectrophotometer at 592 nm and 5 min intervals, and the resulting data were collected during the reaction. The bromination reaction rate constants of the vanadium complexes could be obtained according to the literature method.[30]

Results and discussion

Synthesis discussion

Two vanadium(III) complexes have been successfully synthesized by a hydrothermal reaction at 120 °C (Scheme 1). Because the starting material $V_2(SO_4)_3$(III) is not soluble in common solvents (methanol, ethanol, and water), instead forming a kind of yellow turbid solution in distilled water, we used a hydrothermal reaction at 120 °C to synthesize the complexes. In the synthetic process for the complexes, in order to prevent the metal vanadium(III) center from being oxidized into vanadium(IV) or a higher state, we tried various reducing agents, such as KI, hydrazine hydrochloride, hydrazine hydrate and vitamin C. Finally, we found that vitamin C had the best effect for the synthesis, providing an optimum pH (6.5) and reduction effect. Meanwhile, the temperature of the reaction could not be too high, or the vanadium(III) atom could be oxidized into higher states. In addition, we found that the ethanoyl group of the htba was removed because of the acidic conditions and hot-water backflow.

IR spectral analysis

The IR spectral data of the complexes **1–2** (Fig. S1 and S2, ESI†) are listed in Table S3 (ESI†). It is clear that broad absorption bands appearing at 3417 and 3413 cm^{-1} indicate the presence of water molecules. Absorption occurring at 3274, 3083, and 2973 cm^{-1} should be assigned to the stretching vibrations of C═C–H from the pyrazolyl ring and the benzene ring. The bands at 1623 for **1** and 1672 cm^{-1} for **2** are attributed to the asymmetrical stretching vibration and symmetrical stretching vibration of C═O bonds, respectively. For complex **1**, peaks appear at 1433, 1395, 1209, 1182 and 1076 cm^{-1} because of the stretching vibrations of the pyrazolyl ring. Equivalent peaks are at 1472, 1347, 1224, 1125 and 1060 cm^{-1} for complex **2**. The bands at 934 and 875 cm^{-1} for **1**, and 925 and 878 cm^{-1} for **2** are characteristic of the stretching vibrations of ═C–CH. The bands at 746 and 679 cm^{-1} for **1** and 753 and 684 cm^{-1} for **2** are characteristic of the stretching vibrations of –C–H. The bands at 600 and 562 cm^{-1} for **1** and 585 cm^{-1} for **2** are characteristic of the stretching vibrations of $V–O_{water}$. The bands at 506 cm^{-1} for **1** and 490 cm^{-1} for **2** are attributed to the stretching vibration of $V–O_{carboxyl}$. Absorptions at 477 and 457 cm^{-1} are characteristic of the stretching vibration of V–N.

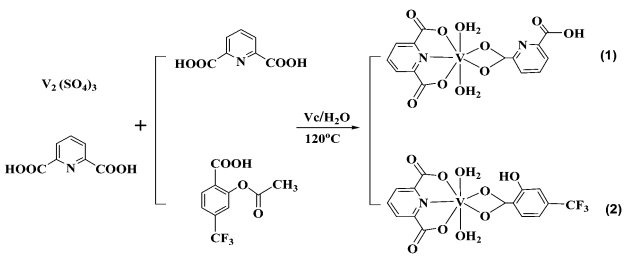

Scheme 1 The reaction processes for the synthesis of the complexes **1** and **2**.

UV-vis spectral analysis

The UV-vis spectra of complexes **1** and **2** (Fig. S3 and S4, ESI†) were recorded for solid state samples, and the characteristic UV-vis bands are listed in Table S4 (ESI†). The complexes have similar absorption patterns. Bands at 274 and 324 nm for **1** and 274 and 320 nm for **2** are attributed to the π–π* transition of the ligands. The bands at 386 nm for **1** and 378 nm for **2** are assigned to the LMCT (ligand to metal charge transfer) transition. The broad peak at 710 nm for **1** and 825 nm for **2** can be caused by the d → d* transition of the central metal vanadium atom.

Structural description of complexes 1–2

$[V(2,6\text{-pdc})_2(H_2O)_2]\cdot 2H_2O$ (1). Structural analysis shows that complex **1** is crystallized in the triclinic system with $P\bar{1}$ space group. The molecular structure of **1** consists of a vanadium atom, two 2,6-pdc ligands, two coordinated water molecules and two free water molecules (Fig. 1). The oxidation state of vanadium is +3. The vanadium atom displays a pentagonal bipyramid geometry; it is coordinated by one nitrogen atom (N1) from a 2,6-pdc ligand, four oxygen atoms (O1, O3, O5, O6) from the 2,6-pdc ligands and two oxygen atoms (O9, O10) from the coordinated water molecules. The two 2,6-pdc ligands adopt tridentate chelating coordination and bidentate coordination modes respectively, with a V–N bond length of 2.123(3) Å. The coordinated water molecules adopt terminal monodentate coordination, and the lengths of the V–O bonds are in the range 2.056(3)–2.139(3) Å. The angles of the N–V–O bonds are in the range 72.99(12)–151.05(12)°. The angle of the O9–V–O10 bonds is 177.10(11)°.

In addition, there are three kinds of intermolecular hydrogen bonds in the structure of complex **1**, as illustrated in Table S2 (ESI†). (i) Hydrogen bonds of O–H···O between the oxygen atoms (O1, O3, O5, O9) from the 2,6-pdc ligands and the oxygen atoms (O9, O10) of the coordinated water (O9–H9B···$O1^{\#1}$: 2.721(4) Å, 162.7°; O9–H9B···$O5^{\#1}$: 3.009(4) Å, 119.5°; O10–H10B···$O3^{\#1}$: 2.787(4) Å, 161.5; O10–H10B···$O6^{\#1}$: 3.016(4) Å, 124.9, #1: $1-x$, $-y$, $1-z$). The molecules are connected to a 1D chain structure by these four hydrogen bond interactions (Fig. 2a). (ii) Hydrogen

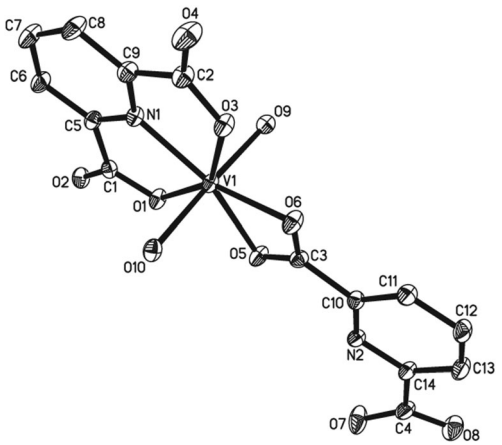

Fig. 1 The molecular structure of **1**.

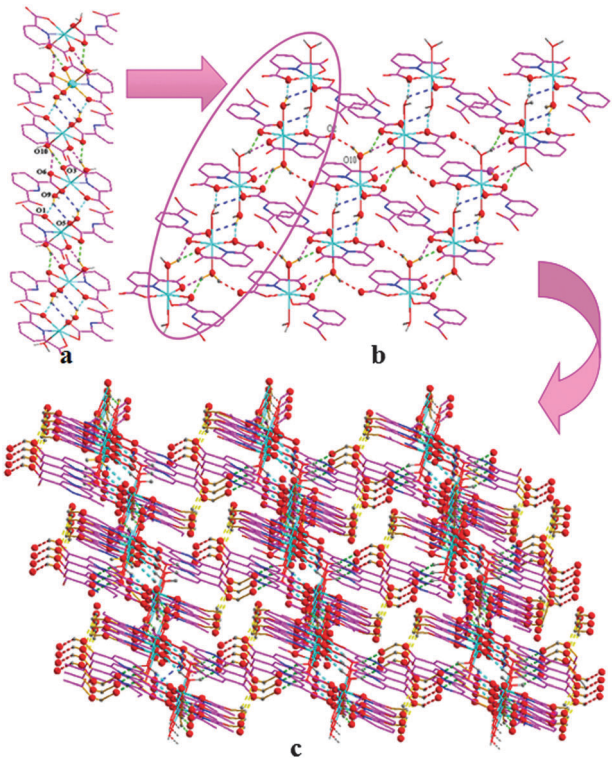

Fig. 2 (a) 1D infinite chain structure of **1**; (b) a view of a 2D supramolecular network structure formed by the hydrogen bonds; (c) the 3D packing framework of the complex **1**.

bonds of O–H···O between an oxygen atom (O2) from the 2,6-pdc ligand and an oxygen atom (O10) from the coordinated water (O10–H10A···O2$^{\#1}$: 2.802(4) Å, 141.9°). Then, the neighbor chains are connected to a 2D sheet structure by the hydrogen bond interactions of O10–H10A···O2$^{\#1}$ (Fig. 2b). (iii) Hydrogen bonds of O–H···O between the oxygen atoms from free water (O1W, O2W) and coordinated water (O9) or 2,6-(pdc) ligands (O4, O8) (O9–H9A···O2W$^{\#1}$: 2.724(4), 158.8°; O8–H8A···O2W$^{\#1}$: 3.240(5), 140.9°; O1W–H1WA···O8$^{\#1}$: 2.785(5), 133.9°; O1W–H1CW···O4$^{\#2}$: 2.780(5), 128.6°, #2 = $1-x$, $1-y$, $1-z$). Finally, the neighbor sheets are connected to a 3D network through four hydrogen bond interactions (Fig. 2c).

V(2,6-pdc)(htba)(H$_2$O)$_2$ (2). Complex **2** crystallizes in the monoclinic system with $P2(1)/c$ space group. The molecular structure of **2** consists of one vanadium atom, one 2,6-pdc ligand, one htba ligand and two coordinated water molecules (Fig. 3). The vanadium atom may be best described as having pentagonal bipyramid geometry; it is coordinated by a nitrogen atom (N) and two oxygen atoms (O5, O7) from the 2,6-pdc ligand, two oxygen atoms (O1, O2) from the htba ligands, and two oxygen atoms (O1W, O2W) from coordinated water molecules. The 2,6-pdc ligand adopts a tridentate chelating coordination mode and the htba ligand adopts a bidentate coordination mode. The bond length of V–N(1) is 2.1050(17) Å. The two coordinated water molecules adopt terminal monodentate coordination; the lengths of V–O are in the range of 2.0339(15)–2.1201(16) Å. The angles of the N–V–O and O–V–O bonds are in the range

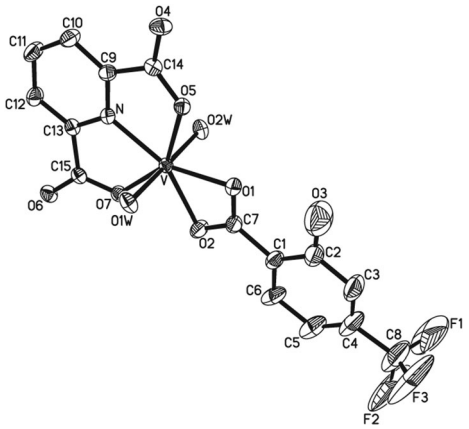

Fig. 3 The molecular structure of **2**.

73.11(6)–149.85(6)° and 61.21(6)–178.69(7)°, respectively. The angle of the O1W–V–O2W is 178.69(7)°.

There are two kinds of hydrogen bonds in the structure of complex **2**. (i) The intermolecular hydrogen bonds of O–H···O between two oxygen atoms (O4, O6, O1W, O2W) from the 2,6-pdc ligand and the coordinated water molecule (O1W–H1W···O4$^{\#1}$: 2.6224(19) Å, 175°; O2W–H2W···O6$^{\#2}$: 2.7187(19) Å, 169°; #1: $1-x$, $1-y$, $1-z$; #2: x, $0.5-y$, $-0.5+z$). The hydrogen bonds O1W–H1W···O4$^{\#1}$ connect the molecules forming a biopolymeric structure (Fig. 4a), and the dipolymers further form a 2D sheet structure with the hydrogen bond O2W–H2W···O6$^{\#2}$ (Fig. 4b). (ii) Intramolecular hydrogen bonds O–H···O between two oxygen atoms from the htba ligand (O3–H3A···O1: 2.588(3) Å, 148.3°), specified as S(6),[34] six atoms forming a closed six-membered ring.

XRD analysis

The powder X-ray diffraction data of the complexes **1** and **2** were obtained and compared with the corresponding simulated single-crystal diffraction data (Fig. S5 and S6, ESI†). The phase of the corresponding complex is considered to be pure owing to

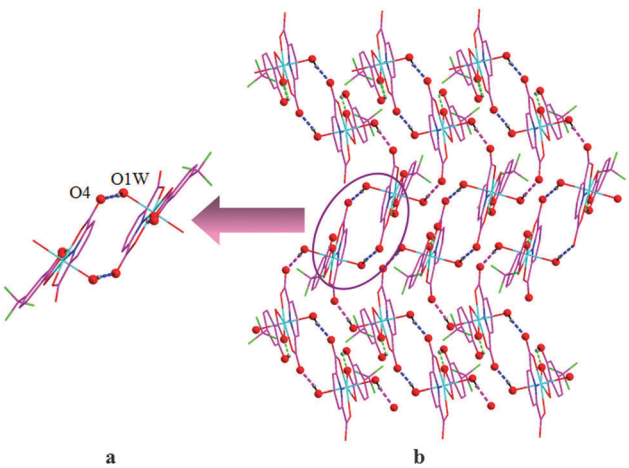

Fig. 4 (a) The biopolymer structure of **2**; (b) a view of a 2D supramolecular network structure formed by the hydrogen bonds.

the agreement of the peak positions. The different intensities may be due to the preferred orientation of the powder samples.

Mimicking the catalytic bromination reaction

To our knowledge, vanadium complexes are able to mimic a reaction in which vanadium haloperoxidases catalyze the bromination of organic substrates in the presence of H_2O_2 and bromide. Herein, the catalytic bromination reaction activities of complexes **1** and **2** were investigated using phenol red as an organic substrate, which is converted to bromophenol blue during the reaction. The reaction is rapid (the maximum reaction rate constant was 2.424×10^2 k(mol L^{-1})$^{-2}$ s^{-1}) and stoichiometric, producing the halogenated product by the reaction of the oxidized halogen species with the organic substrate. The reactive process is shown in Scheme 2.

The addition of a solution of complex **1** to the standard reaction of bromide with phenol red (as a trap for oxidized bromine) in phosphate buffer resulted in the visible color change of the solution from yellow to blue. The electronic absorption spectra recorded a decrease in absorbance of the peak at 443 nm with the loss of phenol red and an increase of the peak at 592 nm with the production of bromophenol blue (shown in Fig. 5).

Complex **1** was used to carry out kinetic studies of the bromination reaction. A series of dA/dt data were obtained (where A = absorbance at 592 nm), changing the concentration of the vanadium complex. Then the plot of $-\log(\mathrm{d}c/\mathrm{d}t)$ *vs.* $-\log c$ for complex **1** (where c = concentration of complex **1**)

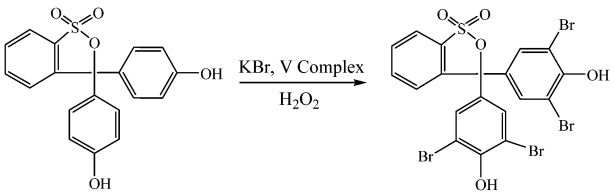

Scheme 2 Reactive process for the bromination reaction of phenol red, catalyzed by the complexes.

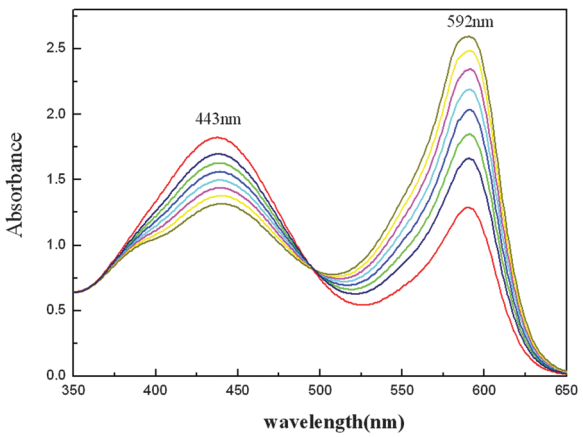

Fig. 5 Oxidative bromination of phenol red catalyzed by **1**. Spectra obtained at 10 min intervals. The reaction mixture contained phosphate buffer (pH 5.8), KBr (0.4 mol L^{-1}), phenol red (10^{-4} mol L^{-1}), H_2O_2 (1 mol L^{-1}) and complex **1** (0.1 mmol L^{-1}).

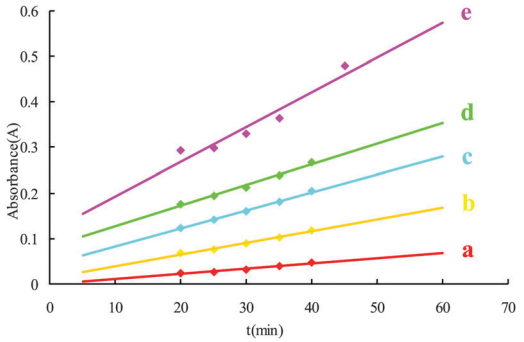

Fig. 6 A series of linear calibration plots showing the dependence of the absorbance at 592 nm on reaction time for different concentrations of complex **1**. Conditions used: pH = 5.8, c(KBr) = 0.4 mol L^{-1}, c(H_2O_2) = 1 mol L^{-1}, c(phenol red) = 10^{-4} mol L^{-1}. c(complex 0.1/mmol L^{-1}) = (a): 1.2×10^{-3}; (b) 2.6×10^{-3}; (c) 4×10^{-3}; (d) 4.5×10^{-3}; (e) 7.6×10^{-3}.

was depicted using the data from Fig. 6, to obtain a straight line (Fig. 7) with a slope of 1.09 and an intercept of 2.0134. The data confirms that the first-order reaction is dependent on vanadium. Based on the equation $b = \log k + y \log c_2 + z \log c_3$, the reaction rate constant, k, is determined by the concentrations of KBr and phenol red (c_2 and c_3), the reaction orders of KBr and phenol red (y and z), as well as b. Since the reaction orders of KBr and phenol red (y and z) are 1 according to the literature, and c_2 and c_3 are known to be 0.4 mol L^{-1} and 10^{-4} mol L^{-1}, respectively, the reaction rate constant (k) for complex **1** can be calculated as 2.424×10^2 (mol L^{-1})$^{-2}$ s^{-1}.

Similar plots for **2** were generated in the same way (Fig. 8 and 9), and values of the slope and the intercept were 1.0048 and 2.2403 respectively.

The cyclic catalytic bromination reaction mechanism is shown in Scheme 3. Centre V atom is coordinated by two water molecules as shown in (a) ([$V(H_2O)_2L_1L_2$]). The vanadium complex easily loses a H_2O forming a compound (b) ([$V(O_2)L_1L_2H_2O$]) with H_2O_2 as an oxidation regent. The formation process of (c) ([$VO_2L_1L_2$]) is the same as that of (b). (c) Is oxidized to form an intermediate compound (d) ([$V(O_2)L_1L_2H_2O$]). Br^- is oxidized rapidly by (d), while at the same time HOBr and (c) are formed with the loss of OH^-. The following process is similar to that in the previous reaction, and the other coordinated water is oxidized with H_2O_2 forming an intermediate (d). Thus (c) oxidizes Br^- into

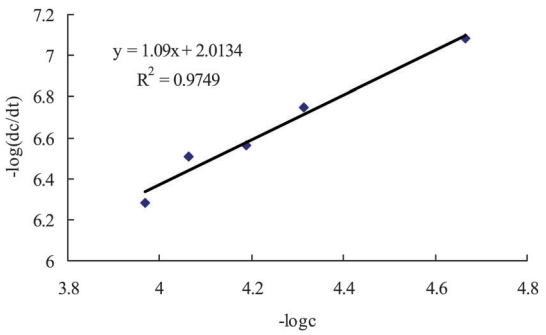

Fig. 7 $-\log(\mathrm{d}c/\mathrm{d}t)$ dependence of $-\log c$ for complex **1** in DMF–H_2O at 30 ± 0.5 °C.

HOBr which further brominates oxidized phenol red. The reaction cycle involving (c) and (d) continues until the phenol red is completely transformed into bromophenol blue.

The experimental results showed that: (i) the reaction orders of the vanadium complexes in the bromination reaction are all close to 1, confirming the first-order dependence of the reaction on vanadium; (ii) the reaction rate constants of the two complexes show the order **1** > **2** (Table 2).

Analysis of the results revealed that the vanadium(III) complexes showed slightly different but high catalytic activity. The order of the reaction rate constant for complexes is **1** > **2**. We thought that the catalytic reaction rate was influenced by the formation of intermediate species. In complex **1**, the bond lengths of V–O between the central metal vanadium atom and coordinated water were 2.076 and 2.070 Å, while they were 2.056 and 3.034 Å in **2**. We know that the longer the bonds are, the weaker the bond energy is. Hence, the V–O bonds in **1** were easier to break to form an intermediate species than those in **2**, so the reaction rate of **1** was faster than that of **2**. Furthermore, there was the same ligand (2,6-pdc) and the same coordination model in the complexes, but the structures differed as a result of the other ligand, 2,6-pdc for **1** and htba for **2**. The space steric effect of htba was bigger than that of 2,6-pdc, because there is a vicinal hydroxyl on the benzene of htba. Therefore, the coordinated H_2O was more easily oxidized to form an intermediate species and so the reaction rate constants showed the order **1** > **2**.

Colorimetric detection of hydrogen peroxide

As we can see, hydrogen peroxide plays an important role in the food industry, clinical medicine, pharmaceutical production and environmental protection, especially because it has great practical effects in catalytic reactions. Based on this view, we studied the effect of the concentration of H_2O_2 upon our catalytic reaction to develop a new H_2O_2 detection method. Through the experimental results, it was found that the oxidation reaction catalyzed by the vanadium complexes is H_2O_2 concentration-dependent, and the absorbance at 592 nm along with the formation of bromophenol blue presents a linear dependence on the concentration of H_2O_2 in a reaction time

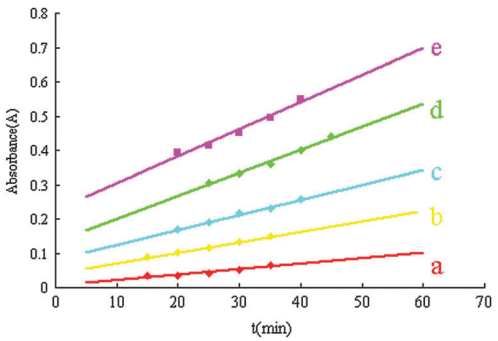

Fig. 8 A series of linear calibration plots showing the dependence of the absorbance at 592 nm dependence on reaction time for different concentrations of complex **2**. Conditions used: pH = 5.8, c(KBr) = 0.4 mol L^{-1}, c(H_2O_2) = 1 mol L^{-1}, c(phenol red) = 10^{-4} mol L^{-1}. c(Complex 0.1/mmol L^{-1}) = (a) 1.6 × 10^{-3}; (b) 3.1 × 10^{-3}; (c) 4.4 × 10^{-3}; (d) 6.7 × 10^{-3}; (e) 7.9 × 10^{-3}.

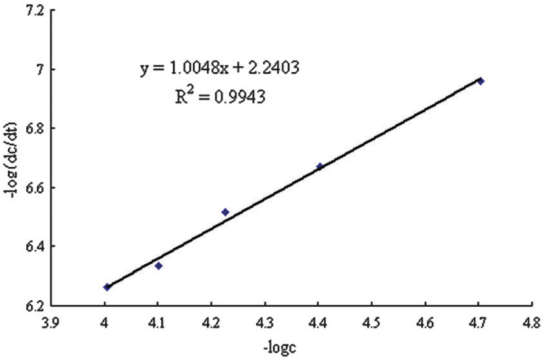

Fig. 9 −log(dc/dt) dependence of −log c for complex **2** in DMF–H_2O at 30 ± 0.5 °C.

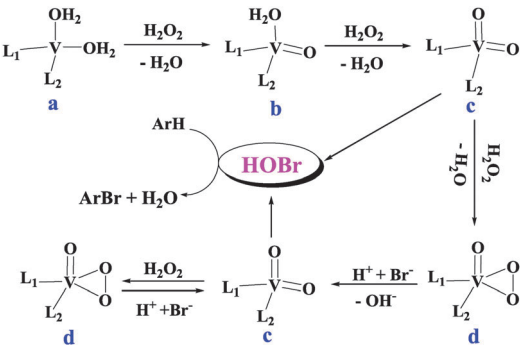

Scheme 3 The cyclic catalytic bromination reaction mechanism.

Table 2 Kinetic data for catalytic bromination by the complexes in DMF–H_2O at 30 ± 0.5 °C[a]

Complexes	m	b	k (mol L^{-1})$^{-2}$ s^{-1}
1	1.09	2.0134	2.424 × 10^2
2	1.00	2.2403	1.437 × 10^2

[a] Conditions used: c(phosphate buffer) = 50 mmol L^{-1}, pH = 5.8, c(KBr) = 0.4 mol L^{-1}, c(phenol red) = 10^{-4} mol L^{-1} "m" is the reaction order of the vanadium complex; "b" is the intercept of the line; "k" is the reaction rate constant for the vanadium complex.

of 25 min (Fig. 10 and 11). The detection limit for the concentration H_2O_2 was estimated to be 0.94 mol L^{-1} for **1** and 0.98 mol L^{-1} for **2** by extrapolation of the graphs. All these observations further confirm that the catalytic reaction system can be used as a potential method for the detection of H_2O_2.

Furthermore, comparisons of the detection limit for complexes reported previously are listed in Table 3. Complexes **3** and **4** were synthesized according to their corresponding ref. 30. **3** is an oxidovanadium(IV) complex with a V=O bond coordinated by a 1,10-phenanthroline and an oxalic acid ligand. **4** is also an oxidovanadium(V) complex with two V=O bonds coordinated by a bpz*T–O ligand (bpz*T–O: 4,6-bis(3,5-dimethylpyrazol-1-yl)-1,3,5-triazin-2-olate). The order of the reaction rate constants for these complexes is **4** > **3** > **2** > **1**. It is found that the **1** and **2** have similar detection limits, which is related to the structure of the complexes. The increasing valence of the

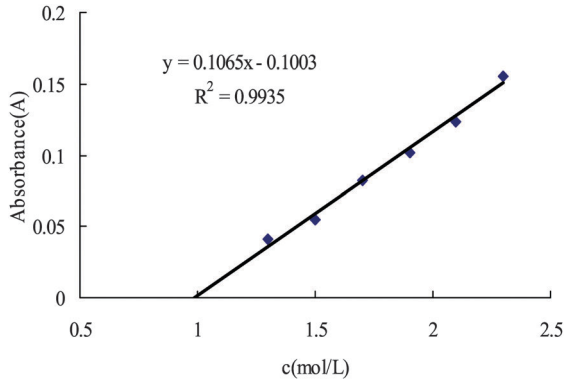

Fig. 10 The linear calibration plot of the absorbance at 592 nm *vs.* the concentration of H_2O_2 in the catalysis reaction of complex **1** in DMF–H_2O at 30 ± 0.5 °C.

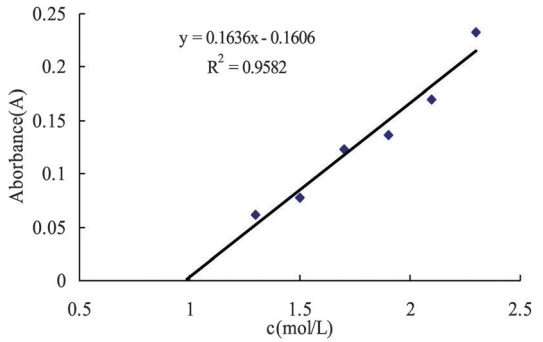

Fig. 11 The linear calibration plot of the absorbance at 592 nm *vs.* the concentration of H_2O_2 in the catalysis reaction of complex **2** in DMF–H_2O at 30 ± 0.5 °C.

Table 3 The detection limits for the complexes

Complexes	LOD (mol L^{-1})
1	0.94
2	0.98
3	1.10
4	1.19

vanadium in complexes **3** and **4** would reduce the selectivity of hydrogen peroxide. Moreover, the coordination mode also has effect on the detection limit, since a higher coordination number would impede the process of the reaction.

Conclusions

Firstly, two new vanadium(III) complexes were successfully synthesized. Structural analysis showed that they have a similar coordination environment and that the vanadium(III) atoms were seven-coordinate with a NO6 donor set in a pentagonal bipyramid geometry. We tested their bromination reaction activities and determined the reaction rate constants (k) of complexes **1** and **2**, which indicated that they can be considered as potential functional models of vanadium haloperoxidases. Furthermore, a new colorimetric detection method for H_2O_2, based on the catalytic bromination reaction was discovered and this detection system was simple and sensitive. We will investigate in detail the application of the detection reaction mechanism in the future.

Acknowledgements

This work was supported by financial assistance from the National Natural Science Foundation of China (Grant No. 21071071, 21371086), and the Commonweal Research Foundation of Liaoning province in China (No. 2014003019).

Notes and references

1 Y. Zuo and J. Hoigné, *Science*, 1992, **260**, 71.
2 A. Tahirovic, A. Copra, E. Omanovic-Miklicanin and K. Kalcher, *Talanta*, 2007, **72**, 1378.
3 (*a*) E. Linley, S. P. Denyer, G. McDonnell, C. Simons and J. Y. Maillard, *J. Antimicrob. Chemother.*, 2012, **67**, 1589; (*b*) W. Chen, S. Cai, Q.-Q. Ren, W. Wen and Y.-D. Zhao, *Analyst*, 2012, **137**, 49; (*c*) T. P. Fellinger, F. Hasché, P. Strasser and M. Antonietti, *J. Am. Chem. Soc.*, 2012, **134**, 4072.
4 (*a*) Z. M. Pei, Y. Murata, G. Benning, S. Thomine, B. Klüsener, J. G. Allen, E. Grill and J. I. Schroeder, *Nature*, 2000, **406**, 731; (*b*) Y. Xiao, H.-X. Ju and H.-Y. Chen, *Anal. Chim. Acta*, 1999, **391**, 73; (*c*) T. Matoba, H. Shimokawa, M. Nakashima, Y. Hirakawa, Y. Mukai, K. Hirano, H. Kanaide and A. Takeshita, *J. Clin. Invest.*, 2000, **106**, 1521.
5 (*a*) K. S waminathan, S. Sandhya, A. C. Sophia, K. Pachhade and Y. V. Subrahmanyam, *Chemosphere*, 2003, **50**, 619; (*b*) H. N. Kim, M. H. Lee, H. J. Kim, J. S. Kim and J. Yoon, *Chem. Soc. Rev.*, 2008, **37**, 1465.
6 J. Wang, Y. Lin and L. Chen, *Analyst*, 1993, **118**, 277.
7 (*a*) P. Niethammer, C. Grabher, A. T. Look and T. Mitchison, *Nature*, 2009, **459**, 996; (*b*) F. Sauer, S. Limbach and G. K. Moortgat, *Atmos. Environ.*, 1997, **31**, 1173; (*c*) M. M. Tarpey and I. Fridovich, *Circ. Res.*, 2001, **89**, 224.
8 (*a*) J. Tang, B. Wang, Z. Wu, X. Han, S. Dong and E. Wang, *Biosens. Bioelectron.*, 2003, **18**, 867; (*b*) A. A. Karyakin, E. E. Karyakina and L. Gorton, *Anal. Chem.*, 2000, **72**, 1720; (*c*) B. C. Dickinson and C. J. Chang, *J. Am. Chem. Soc.*, 2008, **130**, 9638.
9 (*a*) C. Matsubara, K. Kudo, T. Kawashita and K. Takamura, *Anal. Chem.*, 1985, **57**, 1107; (*b*) M. C. Y. Chang, A. Pralle, E. Y. Isacoff and C. J. Chang, *J. Am. Chem. Soc.*, 2004, **126**, 15392; (*c*) E. A. Veal, A. M. Day and B. A. Morgan, *Mol. Cell*, 2007, **26**, 1.
10 S. P. Wolff, *Methods Enzymol.*, 1994, **233**, 182.
11 P. A. Tanner and A. Y. S. Wong, *Anal. Chim. Acta*, 1998, **370**, 279.
12 W. Luo, M. E. Abbas, L. Zhu, K. Deng and H. Tang, *Anal. Chim. Acta*, 2008, **629**, 1.

13 E. W. Miller, O. Tulyanthan, E. Y. Isacoff and C. J. Chang, *Nat. Chem. Biol.*, 2007, **3**, 263.
14 M. J. Navas, A. M. Jimenez and G. Galan, *Atmos. Environ.*, 1999, **33**, 2279.
15 G. De. Faveri, G. Ilyashenko and M. Watkinson, *Chem. Soc. Rev.*, 2011, **40**, 1722.
16 M. Abo, Y. Urano, K. Hanaoka, T. Terai, T. Komatsu and T. Nagano, *J. Am. Chem. Soc.*, 2011, **133**, 10629.
17 (*a*) S. Qian, Y. Chen, L. J. Deterding, Y. C. Fann, C. F. Chignell, K. B. Tomer and R. P. Mason, *Biochem. J.*, 2002, **363**, 281; (*b*) D. H. Bremner, A. E. Burgess, D. Houllemare and K. C. Namkung, *Appl. Catal., B*, 2006, **63**, 15; (*c*) A. H. Vetter and A. Berkessel, *Tetrahedron Lett.*, 1998, **39**, 1741.
18 (*a*) S. Woo, Y. R. Kim, T. D. Chung, Y. Piao and H. Kim, *Electrochim. Acta*, 2012, **59**, 509; (*b*) K. J. Huang, D. J. Niu, X. Liu, Z. W. Wu, Y. Fan, Y. F. Chang and Y. Y. Wu, *Electrochim. Acta*, 2011, **56**, 2947; (*c*) M. Liu, R. Liu and W. Chen, *Biosens. Bioelectron.*, 2013, **45**, 206.
19 (*a*) W. Chen, L. Hong and A.-L. Liu, *Talanta*, 2012, **99**, 643; (*b*) Y. B. Tsaplev, *J. Anal. Chem.*, 2012, **67**, 506; (*c*) W. Shi, X. Zhang, S. He and Y. Huang, *Chem. Commun.*, 2011, **47**, 10785.
20 C. Paul and G. Pohnert, *Nat. Prod. Rep.*, 2011, **28**, 186.
21 (*a*) M. Isupov, A. Dalby, A. Brindley, T. Izumi, T. Tanabe and J. Littlechild, *J. Mol. Biol.*, 2000, **299**, 1035; (*b*) J. Littlechild and E. Garcia-Rodriguez, *Coord. Chem. Rev.*, 2003, **237**, 65.
22 M. Almeida, S. Filipe, M. Humanes, M. F. Maia, R. Melo, N. Severino, J. A. L. da. Silva, J. J. R. Fraústo da Silva and R. Wever, *Phytochemistry*, 2001, **57**, 633.
23 R. Ullrich, J. Nüske, K. Scheibner, J. Spantzel and M. Hofrichter, *Appl. Environ. Microbiol.*, 2004, **70**, 4575.
24 (*a*) A. Butler, *Coord. Chem. Rev.*, 1999, **187**, 17; (*b*) G. R. Nosrati and K. N. Houk, *Biochemistry*, 2012, **51**, 7321; (*c*) M. Sandy, J. N. Carter-Franklin, J. D. Martin and A. Butler, *Chem. Commun.*, 2011, **47**, 12086.
25 (*a*) F. Natalio, R. André, A. F. Hartog, B. Stoll, K. P. Jochun, R. Wever and W. Tremel, *Nat. Nanotechnol.*, 2012, **7**, 530; (*b*) G. E. M. Winter and A. Butler, *Biochemistry*, 1996, **35**, 11805.
26 (*a*) Y.-H. Xing, K. Aoki, F.-Y. Bai, Y.-H. Zhang and B.-L. Zhang, *J. Chem. Crystallogr.*, 2008, **38**, 327; (*b*) N. Teshima, M. Kuno, M. Ueda, H. Ueda, S. Ohno and T. Sakai, *Talanta*, 2009, **79**, 517.
27 Y.-Z. Cao, H.-Y. Zhao, F.-Y. Bai, Y.-H. Xing, D.-M. Wei, S.-Y. Niu and Z. Shi, *Inorg. Chim. Acta*, 2011, **368**, 223.
28 H.-Y. Zhao, Y.-H. Xing, Y.-Z. Cao, Z.-P. Li, D.-M. Wei, X.-Q. Zeng and M.-F. Ge, *J. Mol. Struct.*, 2009, **938**, 54.
29 H.-Y. Zhao, Y.-H. Zhang, Y.-H. Xing, Z.-P. Li, Y.-Z. Cao, M.-F. Ge, X.-Q. Zeng and S.-Y. Niu, *Inorg. Chim. Acta*, 2009, **362**, 4110.
30 C. Chen, Q. Sun, D.-X. Ren, R. Zhang, F.-Y. Bai and Z. Shi, *CrystEngComm*, 2013, **15**, 5561.
31 D.-X. Ren, N. Xing, H. Shan, C. Chen, Y.-Z. Cao and Y.-H. Xing, *Dalton Trans.*, 2013, **42**, 5379.
32 G. M. Sheldrick, *SADABS*, *Program for Empirical Absorption Correction for Area Detector Data*, University of Götingen, Götingen, Germany, 1996.
33 G. M. Sheldrick, *SHELX-97*, *Program for Crystal Structure Analysis*, University of Gottingen, Gottingen, Germany, 1997.
34 J. Bernstein, R. E. Davis, L. Shimoni and N. L. Chang, *Angew. Chem., Int. Ed. Engl.*, 1995, **34**, 1555.

